Supporting Information

Three-dimensional graphene/amorphous porous cobalt molybdenum phosphide nanosheet structure as polysulfide transformation promoters for Li−S batteries

Tongyu Yan[#,a], Hui Zhong[#,a], Wenhao Liao[a], Qingzhou Wu[a], Honghao Ling[a], Xing Liu[a], Huisi Huang[a], Gaixiang Zeng[a], Junsheng Lin[a*]

[a]School of Mechatronic Engineering, Guangdong Meizhou Vocational and Technical College, Meizhou 514028, China

# These authors contributed equally to this work.

[*] Corresponding author: E−mail address: linjunsheng@gdmzvtc.edu.cn.

Experimental section

Synthesis of 3DG

First, a piece of carbon cloth was placed in a tubular furnace, and then heated up to 1100 °C under Ar flow. Subsequently, the tubular furnace was maintained at 1100 °C for 8 h in mixture gas of CH_4/H_2 (V/V=1:9) to grow vertical graphene. Finally, Ar flow was injected and CH_4/H_2 flow was shut off to make the tube furnace cool down naturally to obtained 3DG.

Synthesis of 3DG@Co−MOF

0.657 g of dimethylimidazole and 0.291 g of cobalt nitrate hexahydrate were respectively dissolved in 25 ml of deionized water, then the two solutions were poured into a 100 mL beaker and stirred evenly. A piece of 3DG was placed vertically into the mixed solution. After aging at 25 °C for 5 h, the sample was washed and dried to obtain 3DG@Co−MOF precursor.

Synthesis of 3DG@$CoMoO_4$

Sodium molybdate is dissolved in 50 ml of deionized water to form a transparent solution. Then, a piece of prepared 3DG@Co−MOF was immersed in the solution and held at 100 °C for 3 h. After cooling to 25 °C, the sample was washed and dried to obtain 3DG@$CoMoO_4$-3. 3DG@$CoMoO_4$-2 and 3DG@$CoMoO_4$-4 were obtained through the same process except for changing the reaction time to 2 h and 4 h.

Synthesis of 3DG@CoMoP

A piece of 3DG@$CoMoO_4$ and anhydrous sodium hypophosphite were placed in two separate quartz boats. Anhydrous sodium hypophosphite was located upstream. Then, the quartz boats were transferred to a tubular furnace and heated to 300 °C at a heating rate of 2 °C/min under Ar atmosphere for 1 h to obtain 3DG@CoMoP. In contrast, crystalline 3DG@CoMoP (c-CoMoP) was prepared through the same process except for setting the phosphating temperature to 500 ℃.

Materials characterization

The morphology of the samples were observed using scanning electron microscopy

(SEM, ZEISS Gemini 300) and transmission electron microscopy (TEM, FEI Talos F200X). X−ray diffraction (XRD) tests were investigated by Ultima IV. Raman spectras were performed using Horiba Scientific. The basic elemental composition and chemical valence states were analyzed by X−ray photoelectron spectroscopy (XPS, Axis Ultra DLD Kratos AXIS SUPRA). Brunauer Emmett Teller (BET) analysis was recorded by ASAP2460. Thermogravimetric measurements (TGA) were obtained by TG 209 F1 Libra under air at a heating rate of 5 °C min^{-1}.

Cell Assembly and Electrochemical Measurements

3DG@CoMoP (3DG or CoMoP) was cut into the discs as sulfur host. 0.5 M Li_2S_6 catholyte was added to 3DG@CoMoP to form cathode. The S loading is 3.5 mg cm^{-2}, corresponding to 27 μL of 0.5 M Li_2S_6. The electrolyte was 1.0 M LiTFSI in DOL/DME (V/V = 1:1) with 2 M $LiNO_3$. CR2032 coin cells were assembled using the Li_2S_6/3DG@CoMoP cathode, lithium metal anode, and Celgard 2400 separator. Galvanostatic discharge/charge tests were recorded on the LAND battery test system between 1.7 and 2.8 V. The cyclic voltammetry (CV) tests and electrochemical impedance spectroscopy (EIS) tests were performed on a bio−logic electrochemical workstation.

Adsorption test of lithium polysulfides: Li_2S and sulfur (molar ratio = 1:5) were dissolved in DOL/DME (V/V = 1:1) solution to obtain 0.5 M Li_2S_6 solution. Then, 10 mg 3DG@CoMoP (3DG or CoMoP) were placed in the 10 mL of the diluted Li_2S_6 solutions (5 mM) for 6 h. Finally, the supernatant was selected for UV−Vis adsorption test.

Symmetrical cells tests: 3DG@CoMoP (3DG or CoMoP) was served as working electrodes. Symmetrical cells were assembled using the two identical 3DG@CoMoP electrodes and Celgard 2400 separator. The electrolyte was 1 M LiTFSI and 0.5 M Li_2S_6 in DOL/DME (V/V = 1:1). CV tests were carried out at 10 mV s^{-1} between −1 and 1 V.

Li_2S deposition tests: 3DG@CoMoP (3DG or CoMoP) was directly used as working electrodes. The cell was assembled using 3DG@CoMoP containing 20 μL

Li_2S_8 (0.25 M) and lithium counter electrode containing 20 μL LiTFSI (1 M). The deposition tests of Li_2S were carried out on a Newware battery test instrument. The cell was discharged to 2.06 V at 0.112 mA, and then continuously discharged at 2.05 V until the current is below 0.01 mA.

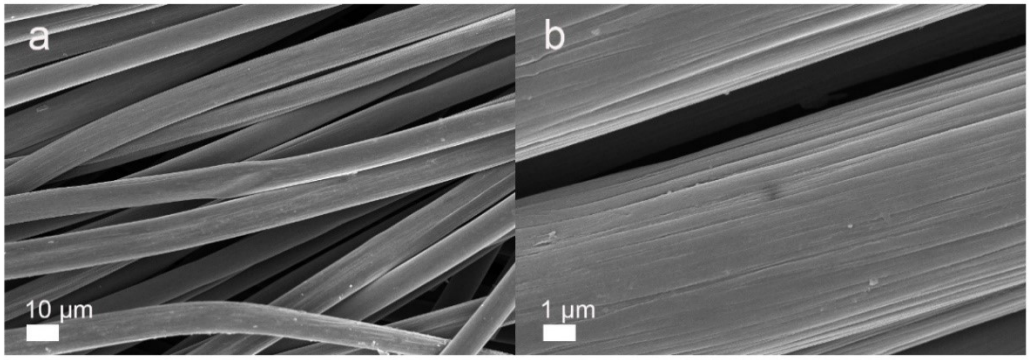

Fig. S1 SEM images of CC.

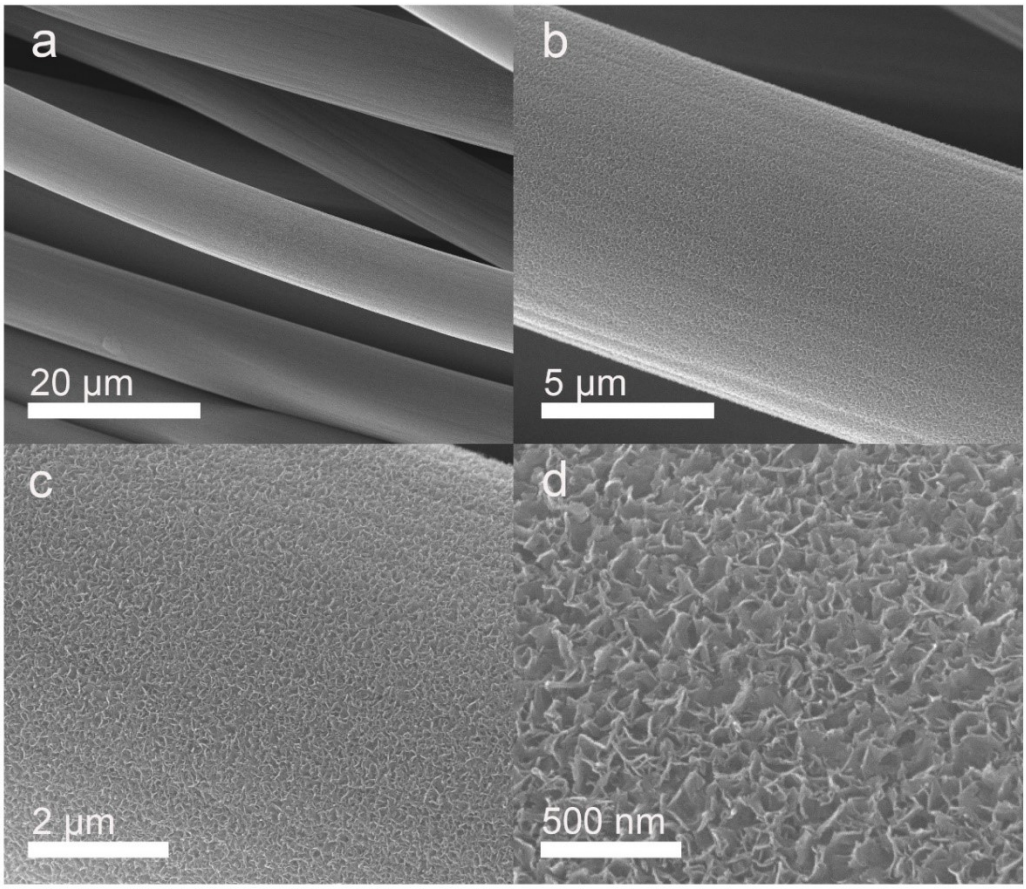

Fig. S2 SEM images of 3DG.

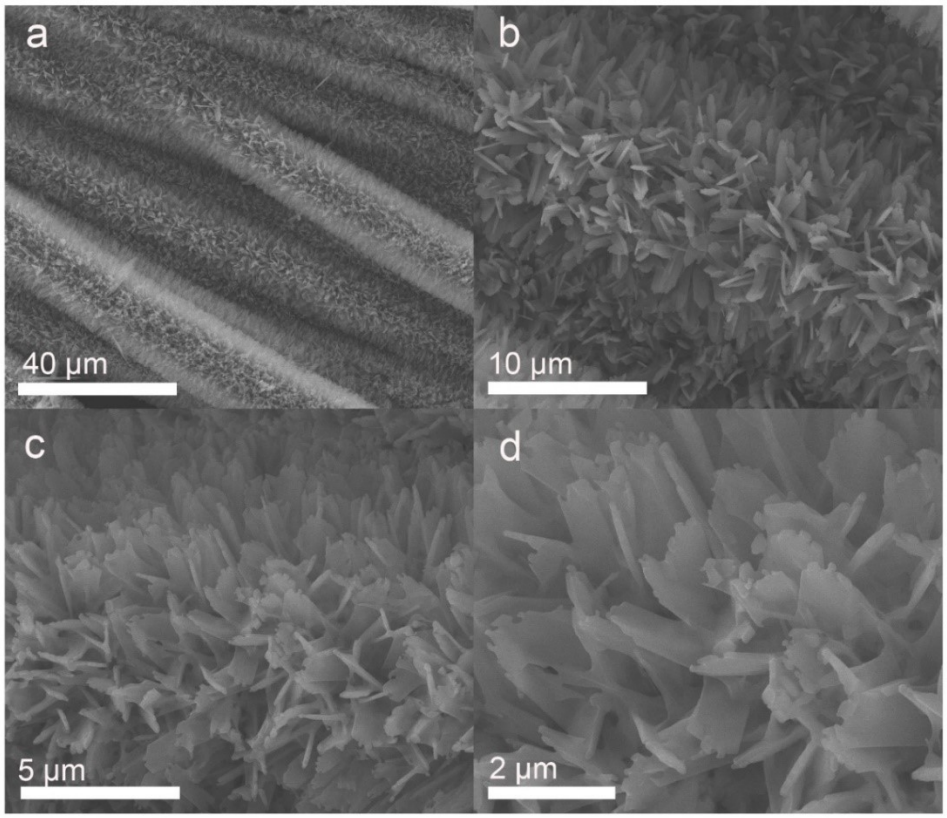

Fig. S3 SEM images of 3DG@Co-MOF.

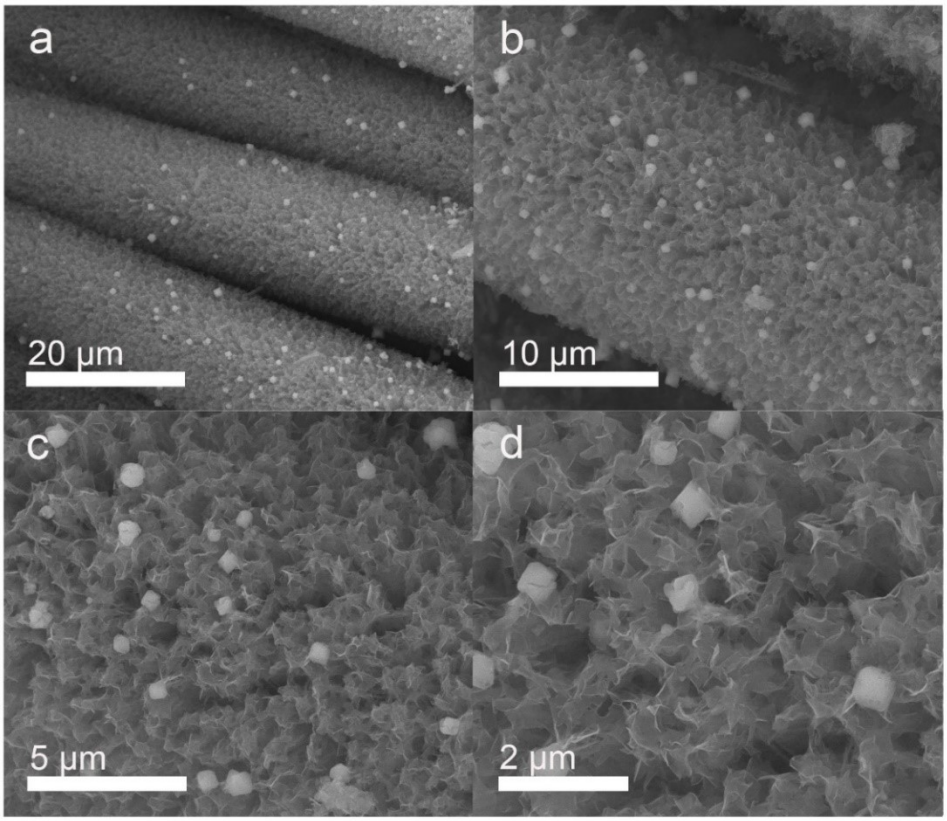

Fig. S4 SEM images of 3DG@$CoMoO_4$-2.

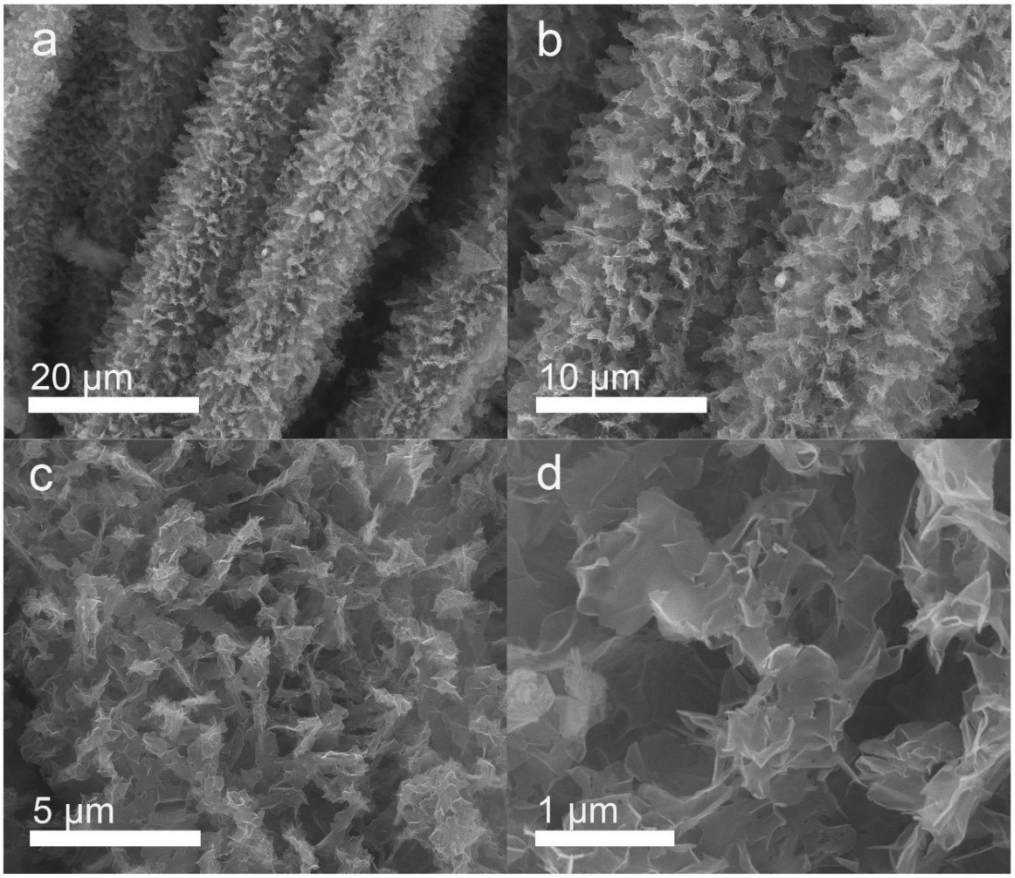

Fig. S5 SEM images of 3DG@$CoMoO_4$-4.

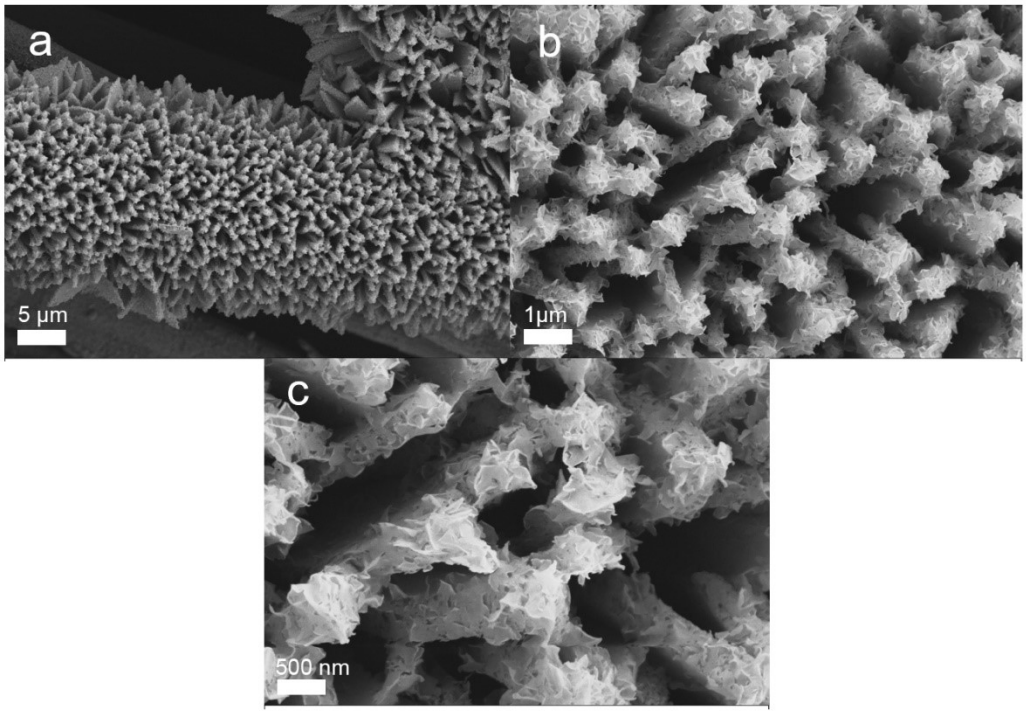

Fig. S6 SEM images of CoMoP.

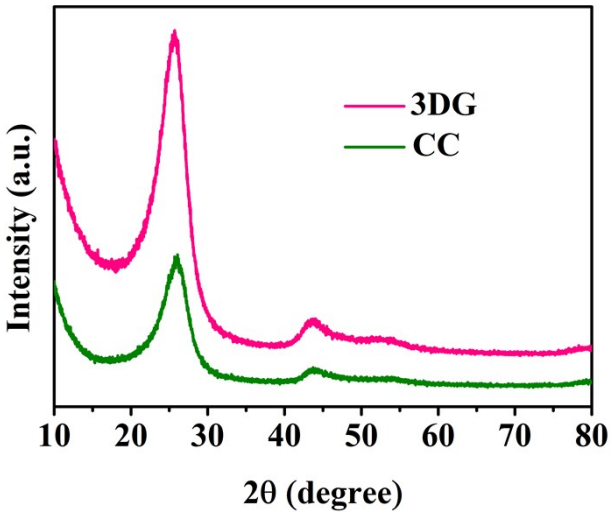

Fig. S7 XRD patterns of CC and 3DG.

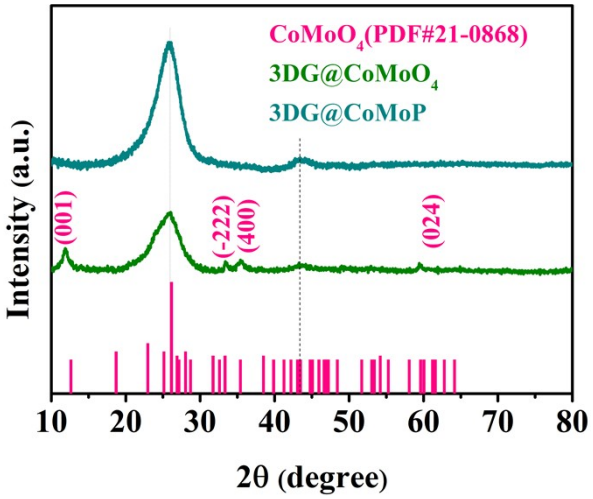

Fig. S8 XRD patterns of 3DG@$CoMoO_4$ and 3DG@CoMoP.

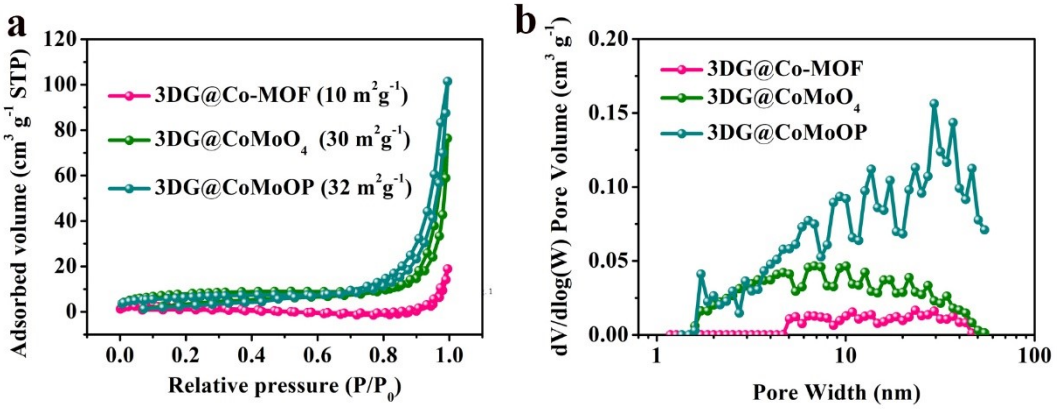

Fig. S9 N_2 adsorption and desorption isotherms (a) and pore size distribution (b) of 3DG@Co-MOF, 3DG@$CoMoO_4$ and 3DG@CoMoP.

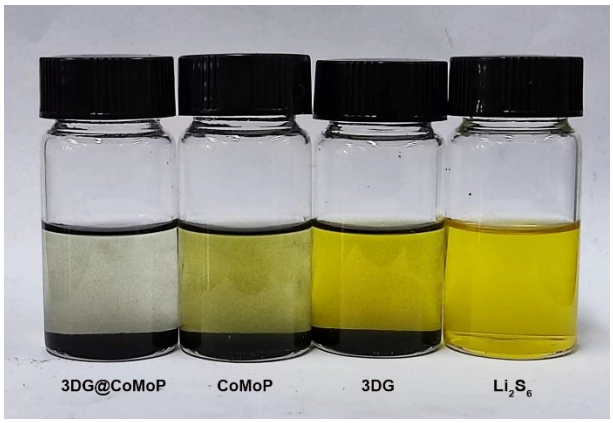

Fig. S10 Images of pristine Li_2S_6 solution and Li_2S_6 solution after adding 3DG, CoMoP and 3DG@CoMoP for 6 h.

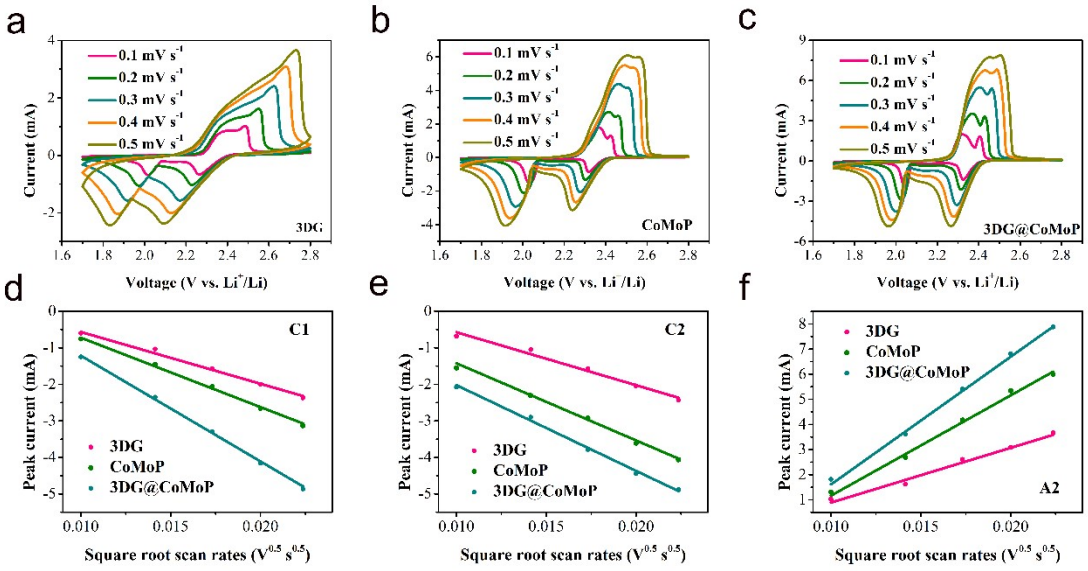

Fig. S11 CV curves (a-c) of the 3DG, CoMoP and 3DG@CoMoP cathodes at different scan rates, (d-f) Plots of peak current vs. the square root of the scan rates.

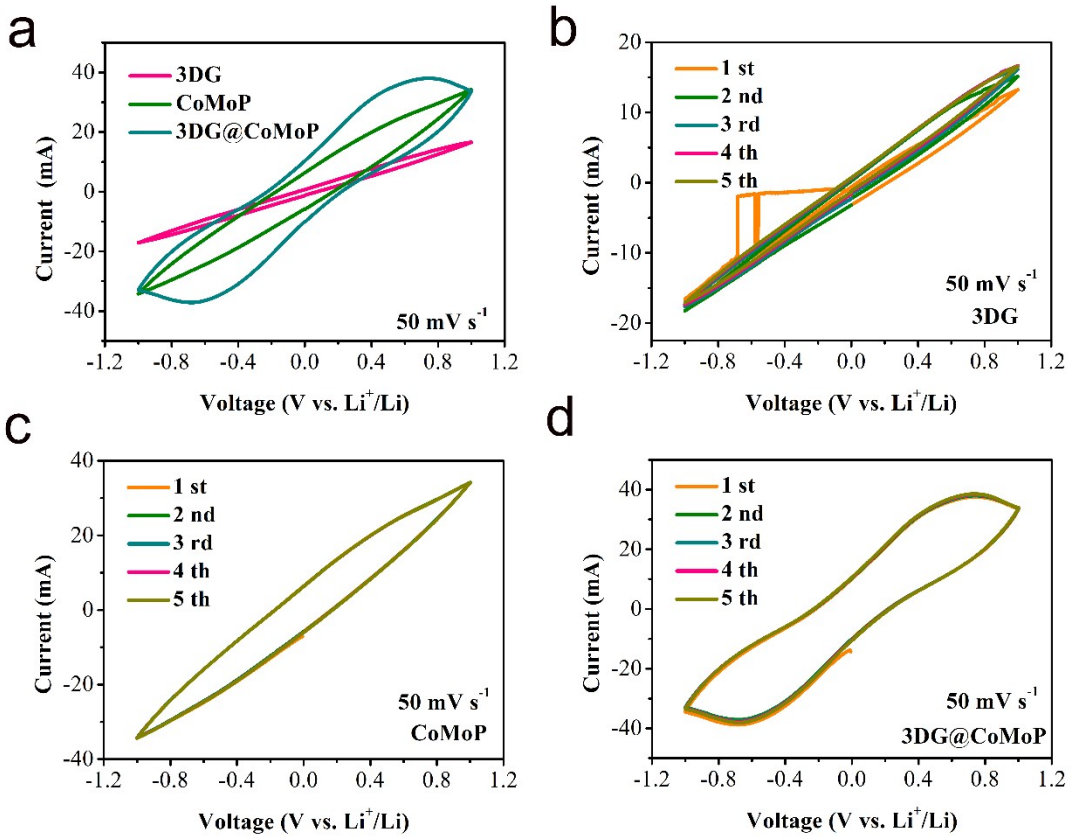

Fig. S12 CV curves of symmetric batteries with 3DG, CoMoP and 3DG@CoMoP electrodes at a scan rate of 50 mV s^{-1}.

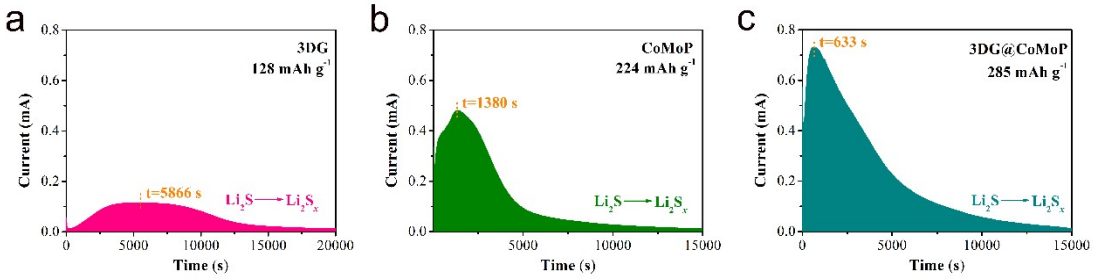

Fig. S13 Li_2S dissolution profiles of 3DG, CoMoP and 3DG@CoMoP.

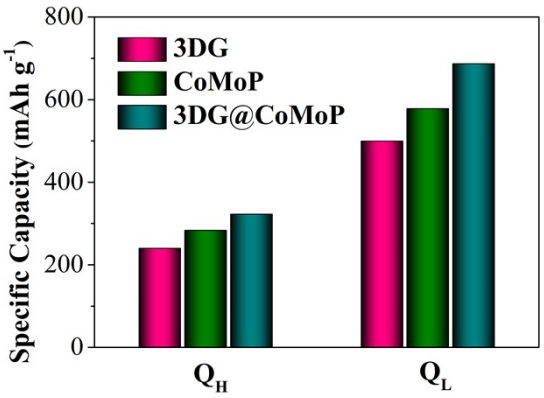

Fig. S14 The comparison of the discharge capacities for upper-platform discharge capacity (Q_H) and lower-platform discharge capacity (Q_L).

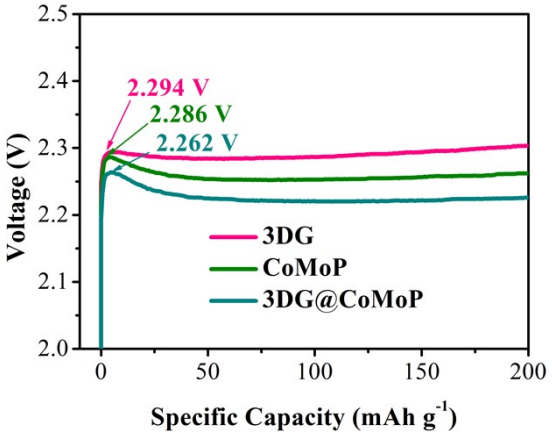

Fig. S15 Charge curves of the 3DG, CoMoP and 3DG@CoMoP cathodes at 0.2 C

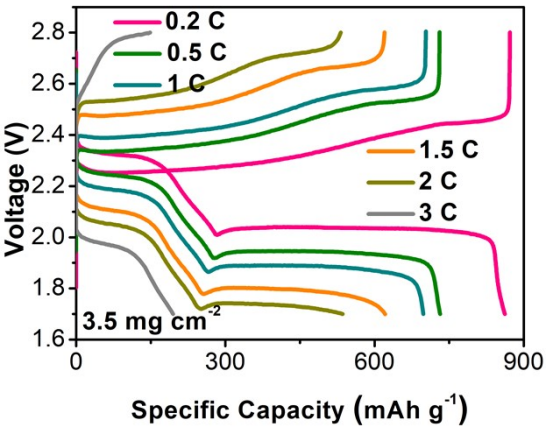

Fig. S16 GCD curves of CoMoP

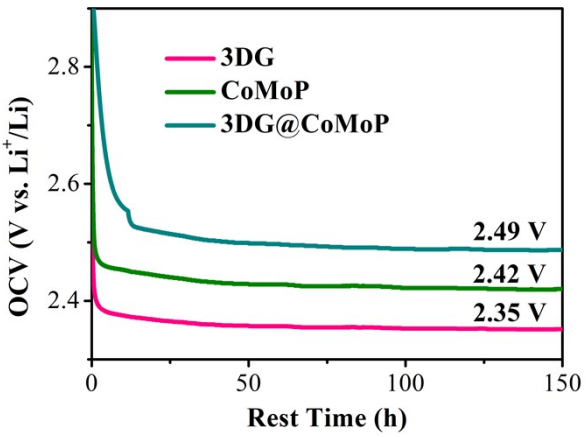

Fig. S17 Self-discharge behavior of the batteries with different cathodes.

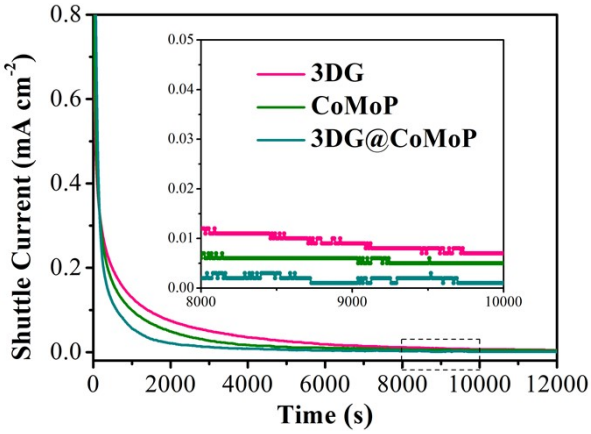

Fig. S18 The shuttle current tests of the batteries with different samples.

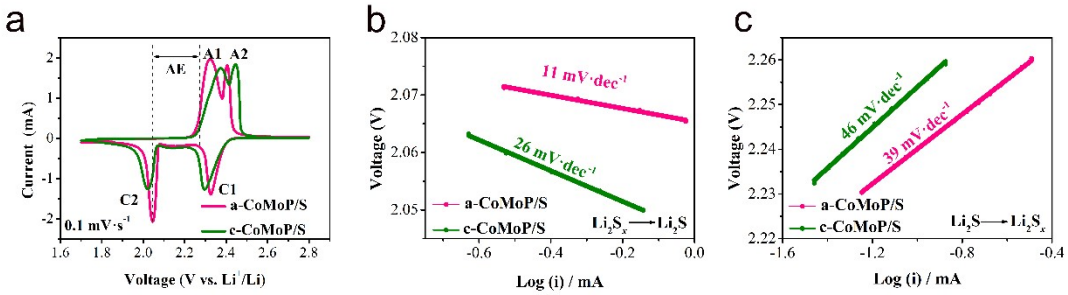

Fig. S19 (a) GCD curves and (b and c) Tafel plots of a-CoMoP and c-CoMoP.

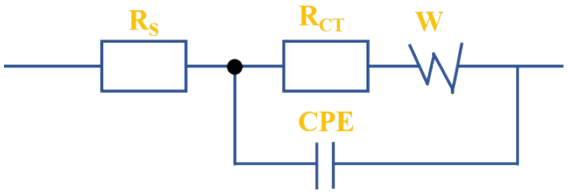

Fig. S20 Equivalent circuit for fitting the electrochemical impedance spectra of the batteries. Rs is the bulk resistance of the batteries. and Rct is the resistance of charge transfer. CPE is a constant phase angle element corresponding to the double-layer capacitance, W is the Warburg impedance related to ion diffusion.

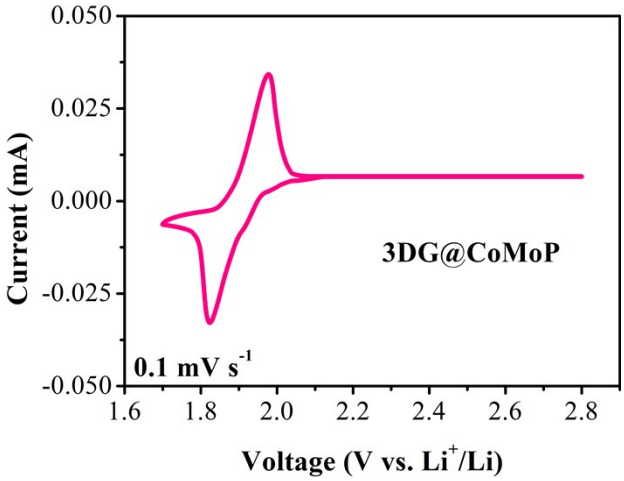

Fig. S21 CV curve at 0.1 mV s^{-1} without active substance sulfur.

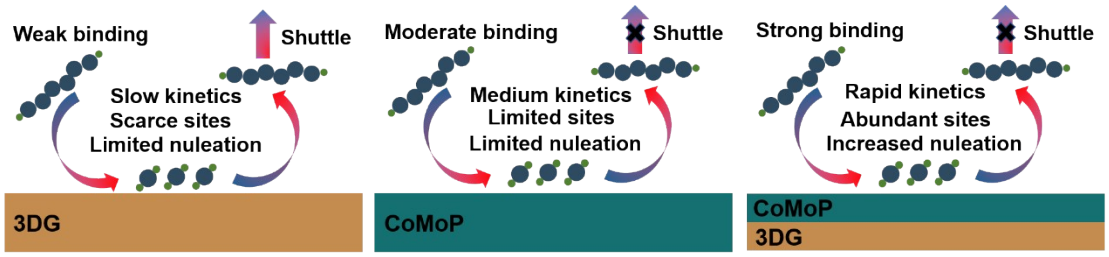

Fig. S22 Schematic illustration of adsorptive and catalytic effect of different structures of 3DG, CoMoP and 3DG@CoMoP on PSs.

Table S1. EIS fitting results of the Li-S batteries with different cathodes.

Sample	Rs (Ω)	Rct (Ω)
3DG	8.97	90.87
CoMoP	8.12	51.54
3DG@CoMoP	8.03	30.35

Table S2 Comparison of areal capacities of 3DG@CoMoP cathode with those of the recent publications in Li-S batteries with high sulfur loading of more than 5 mg cm^{-2}.

materials	Sulfur loading (mg cm^{-2})	Electrolyte/ sulfur ratio (E/S)	Rate (C)	Cycle number	Areal capacity (mAh cm^{-2})	Final capacity (mAh cm^{-2})	Ref.
MoS_3-rGO	8.8	5.5	0.1	100	9.76	7.1	1
FeOOH@CNT	6.2	15	0.1	50	5.74	5.51	2
TiO-NGPC	8.97	18	0.1	100	9.87	9	3
Fe-SNC	7.5	4.7	0.1	100	8	6.06	4
CoFeP@HMCS	8.2	4.87	0.2	200	7.38	6.05	5
MnFe DAC	5	6	0.1	50	4.94	4.57	6
PNKB	7	7	0.1	50	6.63	4.04	7
W/WN@PNCF	7.1	6	0.2	120	5.8	4.8	8
PC-CeO_2	5.5	10.4	0.2	60	7.5	5.6	9
TSI-MOC	9.1	5	0.1	50	9.08	8.32	10
3DG@CoMoP	**9**	**4.8**	**0.1**	**100**	**8.8**	**7.9**	**This work**

References

[1] K. Miao, S. Chen, F. Chen and J. Zhou, *Mater. Rep. Energy*, 2026, DOI: https://doi.org/10.1016/j.matre.2026.100405, 100405.

[2] C. Wei, J. Wang, X. Lei, B. Zhang, L. Wu, L. Tan, Y. Hu, L. Yang, D. Su, X. Wang and Z. Chen, *Nano Energy*, 2025, **146**, 111479.

[3] B. Yu, C. Gyan-Barimah, J. Wang, M. I. Maulana, J. H. Sung, J. H. Yu, S. T. Hong, K. Wang and J. S. Yu, *ACS Nano*, 2025, **19**, 37879-37894.

[4] Y. Cheng, J. Ma, C. Li, Y. Li, H. Li, C. Zhang, J. Yu, S. Cai, F. Wu, J. Zhu, X. Bi, Y. Ren, Y. Xie, Q. Xue, R. He, Z. Li, I. Pinto-Huguet, J. Arbiol, J. Lu, Z. Guo, H. Zhang and A. Cabot, *J. Am. Chem. Soc*., 2025, **147**, 39805-39817.

[5] G. Mu, M. Hu, Z. Cai, J. Xiao, F. Xiao, J. Xi and S. Wang, *J. Energy Chem*., 2026, **113**, 126-135.

[6] S. Won, J. Ji, G. H. Park, S. Kim, S. K. Kang, M. Kim, J. Maeng and W. B. Kim, *J. Energy Chem.*, 2026, **114**, 906-918.

[7] T. Kim, C. Y. Lee, J. Choi, J. Choi, S. Y. Heo, S. E. Kim, K. K. Cho and H. J. Ahn, *ACS Appl. Mater. Interfaces*, 2025, **17**, 65621-65628.

[8] R. Wang, L. Wang, Z. Xu, Q. Liu, M. Cheng, J. Hu, T. Wei, Z. Chen, W. Li and B. Liu, *J. Colloid and Interface Sci.*, 2026, **706**, 139572.

[9] Z. Yang, S. Liu, K. Chen, G. Zhang, F. Gong, S. Xing and J. Wang, *J. Mater. Chem. A*, 2026, DOI: 10.1039/D5TA08719H.

[10] Y. Xiao, H. Lu, Y. Ouyang, J. Yang, J. Rong, J. Weng, Q. Zhang and S. Huang, *ACS Nano*, 2025, **19**, 34858-34868.